A Self-powered Power Management Circuit for Energy Harvested by a Piezoelectric Cantilever

Na Kong[1], Travis Cochran[1], Dong Sam Ha[1], Hung-Chih Lin[2], Daniel J. Inman[1]

[1]Virginia Polytechnic Institute and State University
Blacksburg, VA 24061 USA
{kongna, cochrant, ha, dinman}@vt.edu

[2]National Tsing Hua University,
Hsin-Chu, 30013 TAIWAN
hclin@larc.ee.nthu.edu.tw

***Abstract*-This paper presents development of a self-powered power management circuit for energy harvested by a piezoelectric cantilever. A full-wave rectifier followed by a buck-boost converter running in the discontinuous conduction mode rectifies the AC output, matches the source impedance, and generates a regulated DC output provided the input power is sufficient to charge up the load. A low power microcontroller unit is used for the maximum power point tracking and the output voltage regulation. Experimental results show that the circuit can harvest up to 3.5 mW with a 50x31.8 mm^2 piezoelectric cantilever under 0.5*g* (rms) base acceleration. Detailed loss analysis is presented for efficiency enhancement in the future.**

***Index Terms*- Power management circuit, Energy harvesting, Piezoelectric cantilever**

I. INTRODUCTION

Replacement or recharge of batteries is a major bottleneck for wide deployment of wireless sensor nodes (WSNs), and energy harvested from ambient sources offers a promising solution to the problem [1]-[2]. Energy harvesting for mechanical vibrations is suitable for structural health monitoring, which is the target application of this paper. Vibration-based power generators convert the mechanical energy of vibrating surfaces into electrical energy using a suitable mechanical-to-electrical energy converter (or generator) such as electromagnetic, electrostatic, or piezoelectric transduction devices. We use a piezoelectric cantilever, which offers relatively high power density [3].

Raw electrical power harvested from ambient sources should be conditioned and regulated to a desired voltage level to power up electronic devices. The key design issue for power conditioning circuits is impedance matching. It is complicated as the source impedance depends on the operating conditions. Ottman et al. adopted an adaptive buck converter for impedance matching, but the approach is limited to a harvester whose rectified AC voltage is higher than the output voltage of the system [4]-[5]. Lefeuvre et al. proposed use of a discontinuous conduction mode (DCM) buck-boost converter [6]. Their approach eliminates the previous limitation, but the impedance matching is not guaranteed due to adoption of the open-loop operation (which is intended to reduce the circuit complexity and hence the power consumption). A resonant converter, whose network matches its impedance to the parasitics of the piezoelectric disk, can achieve high efficiency for power conversion [7]-[9]. However, the operating frequency of a piezoelectric transformer is several MHz, which is much higher than a typical vibration frequency of structures (below 200 Hz). To match the impedance of a piezoelectric cantilever, it requires a prohibitively large inductance. Several researchers incorporated switches and inductors to directly shape the output voltage waveform to be in phase with outgoing current [10]-[13]. The non-linear treatment of direct shaping output voltage achieves the maximum power point (MPP) for a certain DC output voltage, which is usually too high for WSNs. So the approach often requires one or two additional voltage regulation stages for WSNs.

This paper presents a self-powered power management circuit, which is capable of handling a wide input voltage range and adjusting the input impedance dynamically through a closed-loop control. The output voltage of the proposed circuit is regulated to power up a WSN provided the input power is sufficient. Loss analysis for the proposed circuit is presented in detail, which can be useful to further enhance the efficiency.

II. THE PROPOSED POWER MANAGEMENT CIRCUIT

A. Source impedance of a cantilevered piezoelectric generator

A piezoelectric energy harvester is typically a cantilevered beam with one or two piezoceramic layers (a unimorph or a bimorph). Figure 1 shows a typical bimorph cantilever configuration [14], where *S* is strain, *V* voltage, *M* mass, and *z* vertical displacement. A mass is placed on the free end to tune the resonant frequency of the system. The two piezoceramic layers are poled oppositely along the 3 axis and electrodes are placed on the surfaces perpendicular to the 3 axis. The beam undergoes bending vibrations due to the motion of its base, and the driving vibrations are assumed to exist only along the 3 axis. Under the assumptions, the piezoelectric material experiences a one-dimensional state of stress along the 1 axis. Then, the dynamic strain induced in the piezoceramic layers generates an AC voltage output across the electrodes.

The equivalent circuit for the first vibrational mode of a bimorph piezoelectric cantilever is shown in Figure 2 [15].

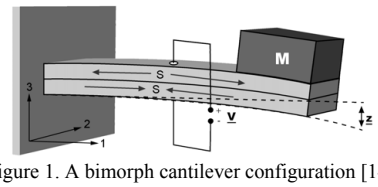

Figure 1. A bimorph cantilever configuration [14].

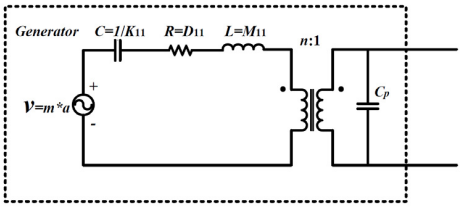

Figure 2. The equivalent circuit for the first mode piezoelectric generator.

The voltage generator $v = m^*a$ represents the force induced by the base vibration and is the only source in the electrical model, where m^* is the effective modal forcing term and a is the base acceleration amplitude. The equivalent inductor $L = M_{11}$ represents the modal mass of the first mode. The resistor $R = D_{11}$ and the capacitor $C = 1/K_{11}$ represent mechanical damping and compliance (reciprocal of stiffness), respectively. The electromechanical coupling is modeled as a transformer with the turns ratio of n. C_P is the equivalent inherent capacitance of the piezoceramic layers.

The equivalent source impedance is shown in Figure 3. The resonance frequency of the generator is usually tuned to match the vibration frequency of the base structure. In this case, the resistive load which matches the source impedance extracts maximal power.

B. Operation of the impedance matching circuit

Figure 4 shows the circuit diagram. A full-wave rectifier rectifies the AC output. A buck-boost converter running in the DCM is chosen for the second stage to

(i) accommodate a wide range of input voltage; and

(ii) behave as a lossless resistor to match the source impedance for the maximum power point tracking (MPPT) [16].

An ultra-low power microcontroller unit (MCU) MSP430 from Texas Instruments is configured to provide the MPPT and the output voltage regulation. A supercapacitor is chosen as a storage device for our system due to a less strict requirement for charging and virtually unlimited charging and discharging cycles. A backup battery is added for the initial start of the circuit (specifically for the MCU) as well as backup power in case of insufficient input power.

Waveforms for a half cycle of a harmonic base vibration are shown in Figure 5. The waveform of the rectified voltage v_{rect} is approximately sinusoidal with the peak value of $V_{in,peak}$. Since the base vibration frequency F_v is much lower (about 44 Hz for our case) than the switching frequency $F_S = 1/T_S$ (about 3 kHz), the input voltage to the buck-boost converter is assumed as DC voltage for each switching period T_S. The effective input resistance of the buck-boost converter is obtained as (1).

$$R_{in} = \frac{v_{rect}}{\frac{1}{T_S}\int_0^{D_1 T_S} i_L dt} = \frac{v_{rect}}{\frac{1}{T_S}\int_0^{D_1 T_S} \frac{v_{rect}}{L} tdt} = \frac{2L}{D_1^2 T_s} \quad (1)$$

In order to achieve the resistive impedance matching, the effective input resistance R_{in} should be equal to the optimal resistive load $R_{in,opt}$ given in (1). Hence, the optimal duty cycle can be expressed as

$$D_{1,opt} = \sqrt{\frac{2L}{R_{in,opt} T_s}} . \quad (2)$$

The maximum inductor current $I_{L,\max}$ and the first off-time D_2 during each switching cycle can also be assumed sinusoidal, i.e.

$$I_{L,\max}(n) = I_{L,\max,peak} \left|\sin(2\pi F_v (n-1+D_1) T_s)\right| , \quad (3)$$

where $n = 1, 2, ...; I_{L,\max,peak} = V_{in,peak} D_1 T_s / L$;

$$D_2(n) = D_{2,peak} \left|\sin(2\pi F_v (n-1+D_1) T_s)\right| , \quad (4)$$

where $n = 1, 2, ...; D_{2,peak} = I_{L,\max,peak} L / V_o T_s$.

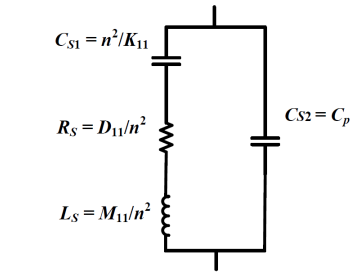

Figure 3. Equivalent source impedance of a piezoelectric generator.

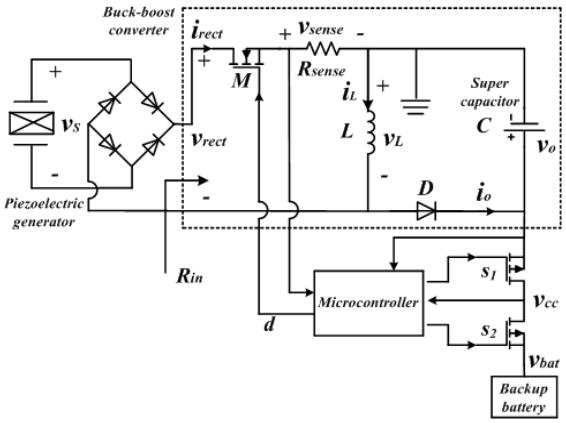

Figure 4. Circuit diagram of the self-powered energy harvesting system.

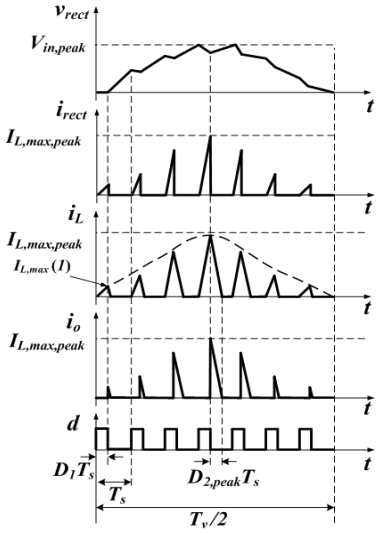

Figure 5. Waveforms during half cycle of a harmonic base vibration.

III. MPPT AND VOLTAGE REGULATION

Instead of adopting multiple power conversion stages, we propose to use a single power stage with two different operation modes – MPPT and output voltage regulation – depending on the output voltage of the supercapacitor or the charge level of the supercapacitor. When the supercapacitor is charged initially, the capacitor voltage is lower than a predetermined high threshold voltage V_{HT}. The control loop adjusts the duty cycle of the switches to achieve the MPPT. When the output voltage reaches above V_{HT}, the MPPT control loop turns off, and another control loop turns on to regulate the output voltage of the supercapacitor. The status implies that it has harvested sufficient energy, and so it adjusts the duty cycle to regulate the output voltage rather than the impedance matching. When the input power harvested is insufficient, the output voltage decreases and eventually becomes lower than another a predetermined low threshold voltage V_{LT} (which is lower than V_{HT}). Then, the MPPT control loop turns on to maximize power harvesting through the MPPT.

The optimal duty cycle $D_{1,opt}$ corresponding to the maximum power point is obtained in (2). Based on the circuit parameters used for our experiments (to be given in Section V), the optimal duty cycle is around 3.5% or 10 μs switch on-time for the switching frequency of 3.5 kHz. 1% change of the optimal duty cycle (ΔD = 0.035%) for the traditional constant switching frequency modulation scheme requires ΔT_{on} = 100 ns, which in turn requires 10 MHz of the clock frequency. In contrast, the - 1% change of duty cycle (ΔD = -0.035%) for the constant on-time modulation requires ΔT_{off} = -2.6 μs), which can be achieved with 385 kHz of the clock frequency. The constant on-time modulation reduces the clock frequency by a factor around 26 compared with the constant switching frequency modulation, and is adopted for our circuit. The optimal switching frequency for a fixed switch on-time T_{on} can be derived from (2) and is given as

$$F_{S,opt} = \frac{2L}{T_{on}^2 R_{in,opt}} \tag{5}$$

For each switching cycle, the input power charges the inductor during switch on-time and releases the inductor energy fully to the load due to the DCM operation. Therefore, the average power delivered to the load for each switching cycle can be expressed as in (6).

$$P_{avg} = \frac{1}{2} L I_{L,\max}^2 F_S \tag{6}$$

Sensing only the inductor current is sufficient to obtain the average power harvested by the buck-boost converter. The constant on-time modulation makes it simple to sense the inductor current at the middle point of the switch on-time, which avoids sensing the noisy peak current.

Control-loop adjusts the switching period T_S to achieve the MPPT using hill-climbing method [17]-[18]. The detailed operation of the MPPT algorithm is shown in Figure 6. The switch on-time is fixed T_{on} and the initial switching period is perturbed with a small decrease. Since the maximum inductor current $I_{L,\max}$ is sinusoidal, the controller looks for the peak of

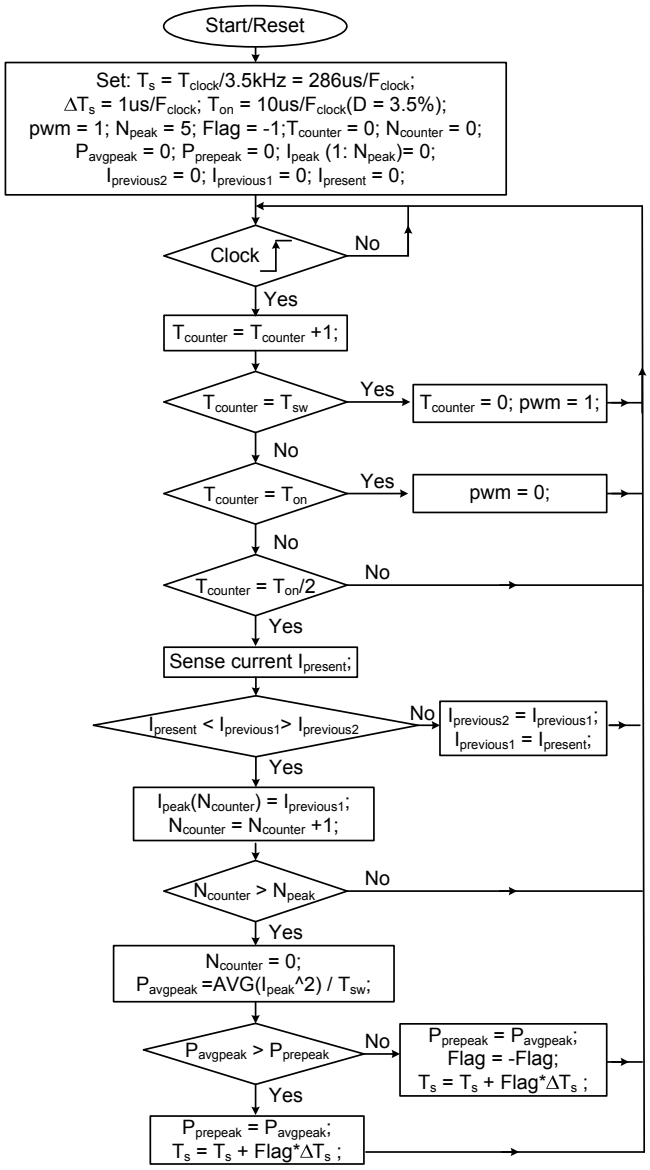

Figure 6. Flow chart of the MPPT algorithm.

the sinusoidal waveform and use (6) to calculate the average input power. To overcome the errors caused by noises, the calculation of average input power takes an average of five consecutive values. If the average input power increased, the switching period keeps decreasing; otherwise the switching period is increased. The hill-climbing process continues. Finally, the switching period will stable around the optimal operation point. Once the circuit reaches at the MPP, the controller runs at a low clock frequency to save power and updates its switching period less frequently.

IV. ANALYSIS OF POWER LOSSES

In order to figure out the sources of power dissipation, the losses in the proposed system are analyzed in this section. The target application for the proposed power management circuit

is structural health monitoring, in which a sensor node is activated at a low duty cycle such as once or a few times a day. So, the load for the proposed power management circuit is assumed idle for our loss analysis. Further, the circuit is assumed in the steady state, in which the resistive impedance matching has achieved already by adjusting the switching period T_S.

Under the assumptions given above, the waveform of the rectified voltage V_{rect} is approximately $V_{in,peak}|\sin(2\pi F_v t)|$, where $V_{in,peak}$ is the peak voltage of the piezoelectric generator and F_v is the base vibration frequency. Also, the envelops of inductor current i_L and the super capacitor charge current i_o are approximately sinusoidal. The major power losses are due to power dissipation of six components – the full-bridge rectifier, the MOSFET M, the diode D, the inductor L, the sensing resistor R_{sense} and the MCU. Refer to Figure 4 and Figure 5 for notations used in expressions given below.

A. Rectifier

The first-order forward voltage drop of a diode is expressed as $v_F = \mathrm{k}i_L + \mathrm{b}$, where i_L is the forward current and k and b are two constants, and the power loss of a diode is $\mathrm{v}_F \times i_L$. During the switching cycle corresponding to the inductor current $I_{L,\max}$ achieving the peak value $I_{L,\max,peak}$, the average conduction loss of the rectifier in this switching cycle can be calculated as

$$\begin{aligned} &P_{cond,rectifier,peak} \\ &= \frac{2}{T_s}\int_0^{D_1 T_s} V_F i_L dt \\ &= \frac{2}{T_s}\int_0^{D_1 T_s}\left(k\left(\frac{I_{L,\max,peak}}{D_1 T_s}t\right)^2 + b\frac{I_{L,\max,peak}}{D_1 T_s}t\right)dt \\ &= 2D_1\left(\frac{k}{3}\left(I_{L,\max,peak}\right)^2 + \frac{b}{2}I_{L,\max,peak}\right) \end{aligned} \quad . \tag{7}$$

So the average conduction loss of the rectifier in the vibration cycle can be calculated as

$$\begin{aligned} &P_{cond,recfitier} \\ &= \frac{2}{T_v}\int_0^{\frac{T_v}{2}} 2D_1\left(\frac{k}{3}\left(I_{L,\max,peak}\sin(2\pi F_v t)\right)^2 + \frac{b}{2}\left(I_{L,\max,peak}\sin(2\pi F_v t)\right)\right)dt \\ &= 2D_1\left(\frac{k}{6}\left(I_{L,\max,peak}\right)^2 + \frac{b}{\pi}I_{L,\max,peak}\right) \end{aligned} \quad . \tag{8}$$

Smaller D_1 and/or $I_{L,\max,peak}$ reduces the loss, but it degrades the system performance. Smaller k and b can be achieved by using higher performance diodes.

B. MOSFET M

Similarly, the conduction loss can be obtained as:

$$\begin{aligned} &P_{cond,mosfet,peak} = \frac{1}{T_s}\int_0^{D_1 T_s} i_L^2 R_{ds,on} dt \\ &= \frac{1}{T_s}\int_0^{D_1 T_s}\left(\frac{I_{L,\max,peak}}{D_1 T_s}t\right)^2 R_{ds,on} dt \\ &= \frac{D_1}{3}\left(I_{L,\max,peak}\right)^2 R_{ds,on} \end{aligned} \quad , \tag{9}$$

$$\begin{aligned} &P_{cond,mosfet} \\ &= \frac{2}{T_v}\int_0^{\frac{T_v}{2}} P_{cond,mosfet,peak}\sin^2(2\pi F_v t)dt \\ &= \frac{1}{2}P_{cond,mosfet,peak} \end{aligned} \quad . \tag{10}$$

where $R_{ds,on}$ is the drain-source on-resistance of the MOSFET. Many factors such as the gate-source voltage V_{GS} and the drain current I_D affect $R_{ds,on}$.

The switching loss is due to voltage-current overlap during the turning-off transition and the loss on output capacitance during the turning-on transition.

$$\begin{aligned} &P_{switching,mosfet} \\ &= \frac{1}{2}P_{switching,mosfet,peak} \\ &= \frac{1}{2}\left(\frac{1}{2}V_{in,peak}I_{L,\max,peak}t_f + \frac{1}{2}C_{oss}\left(V_{in,peak}\right)^2\right)F_s \end{aligned} \tag{11}$$

where F_s is the switching frequency, t_f is the falling time of the gate input signal, and C_{oss} denotes the output capacitance of the MOSFET. Reduction of t_f and C_{oss} decrease the switching loss without direct affect on the performance, but other parameters do affect.

C. Diode D

The current going through the diode is the off-time inductor current. Similar to the rectifier:

$$\begin{aligned} &P_{cond,diode,peak} \\ &= \frac{1}{T_s}\int_0^{D_{2,peak}T_s} V_F i_L dt \\ &= \frac{1}{T_s}\int_0^{D_{2,peak}T_s}\left(k\left(\frac{I_{L,\max,peak}}{D_{2,peak}T_s}t\right) + b\right)\frac{I_{L,\max,peak}}{D_{2,peak}T_s}t dt \\ &= D_{2,peak}\left(\frac{k}{3}\left(I_{L,\max,peak}\right)^2 + \frac{b}{2}I_{L,\max,peak}\right) \end{aligned} \quad ; \tag{12}$$

$$\begin{aligned} &P_{cond,diode} \\ &= \frac{2D_{2,peak}}{T_v}\int_0^{\frac{T_v}{2}}\left(\frac{k}{3}\left(I_{L,\max,peak}\right)^2\left(\sin(2\pi F_v t)\right)^3 + \frac{b}{2}I_{L,\max,peak}\left(\sin(2\pi F_v t)\right)^2\right)dt \\ &= D_{2,peak}\left(\frac{4k}{9\pi}\left(I_{L,\max,peak}\right)^2 + \frac{b}{4}I_{L,\max,peak}\right) \end{aligned} \quad . \tag{13}$$

The switching loss of the diode is only due to the turning-on activity.

$$P_{switching,diode,peak} = \frac{1}{2}C_j\left(V_o + V_{in,peak}\right)^2 F_s \tag{14}$$

$$P_{switching,diode} = \frac{1}{2}C_j\left(V_o^2 + \frac{4}{\pi}V_o V_{in,peak} + \frac{1}{2}\left(V_{in,peak}\right)^2\right)F_s \tag{15}$$

where C_j is diode capacitance.

D. Inductor L

The loss is due to the parasitic resistance R_{dcr}, and occurs both during on- and off-times.

$$P_{cond,ind,peak} = \frac{1}{T_s}\int_0^{T_s} i_L^2 R_{dcr}\,dt = \frac{1}{3}\left(I_{L,\max,peak}\right)^2 R_{dcr}\left(D_1 + D_{2,peak}\right) \quad (16)$$

$$P_{cond,ind} = \frac{1}{3}\left(I_{L,\max,peak}\right)^2 R_{dcr}\left(D_1\left(\frac{2}{T_v}\int_0^{\frac{T_v}{2}} \sin^2(2\pi F_v t)dt\right) + D_{2,peak}\left(\frac{2}{T_v}\int_0^{\frac{T_v}{2}} \sin^3(2\pi F_v t)dt\right)\right) = \frac{1}{3}\left(I_{L,\max,peak}\right)^2 R_{dcr}\left(\frac{1}{2}D_1 + \frac{4}{3\pi}D_{2,peak}\right) \quad (17)$$

E. Sensing resistor

Conduction loss is similar to R_{dcr} of the inductor, but it occurs only during on-time.

$$P_{cond,Rsense} = \frac{1}{6}\left(I_{L,Max,peak}\right)^2 R_{sense} D_1 \quad (18)$$

F. Controller

It is mainly attributed to the power dissipated by the MCU. The loss of the controller is hard to analyze, so we rely on actual measurements.

V. Experimental Results

To verify the feasibility of the proposed circuit, experiments were performed using a cantilevered bimorph generator with a tip mass. The bimorph (manufactured by Piezo Systems, Inc. with model number T226-A4-503X) consists of two oppositely poled PZT-5A piezoelectric elements bracketing a brass substructure layer, and the two piezoelectric elements are connected in series. The base acceleration applied to the piezoelectric cantilever is 0.5*g* (rms) for the experiment. The optimal resistive load of the piezoelectric cantilever for a given frequency is the one which maximizes the average power output and was identified by tuning the load resistor. The experimental result is shown in Figure 7. The optimal resistor is 60 kΩ at the resonant frequency of 44 Hz in the figure.

The experiment setup to measure the performance of the power management circuit is shown in Figure 8. The electrical components used for the circuit are listed in Table I. The load of the circuit is a wireless sensor board (which is a TI MSP430 MCU evaluation board configured for structural health monitoring) with supply voltage of 3.5 V. Figure 9 shows the measured current going into the MCU (top), the charging profile of the supercapacitor and the supply voltage of the MCU (bottom) under 0.5*g* (rms) base acceleration . The MCU is in the active mode for 0.4 second and returns to sleep mode for 13 seconds. It consumes 3.5 mA in the active mode and 175 μA during the sleep mode. The top graph in Figure 9 shows sharp differences in current during the two different modes. The bottom graphs indicate that the circuit is in the MPPT mode for the first 210 seconds. The output voltages of the supercapacitor and the MCU rise continuously during the mode. When the two voltages reach around 3.5 V, the circuit switches to the voltage regulation mode and tries to maintain the voltage.

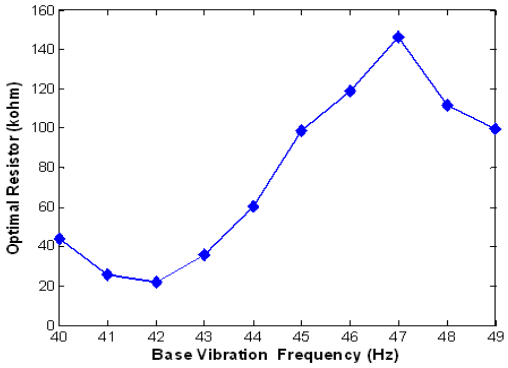

Figure 7. Optimal resistance versus excitation frequency.

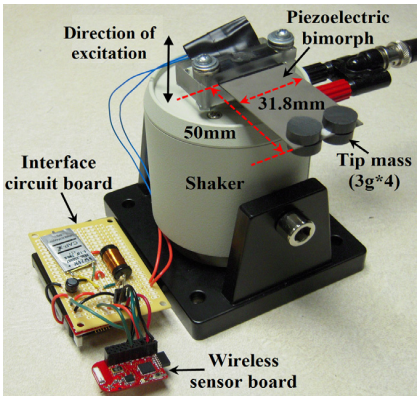

Figure 8. The experiment setup

Table I. Converter parameters

Component	Part Number	Notes
Rectifier	BAS3007	V_F =0.32V@10mA, 0.4V@ 100 mA.
MOSFET	2N7002	R_{dson} =5.3 Ω@V_{GS} = 4.5V;C_{oss}=40 pF.
Schottky Diode	PMEG4005	V_F=0.27mV@10mA,0.35V@100mA.
Inductor L	102K1R3	L = 10 mH; DCR = 9.1 Ω.
Super capacitor C	GW209F	C = 0.12 F; ESR = 70 mΩ.
Rsense	--	10 Ω

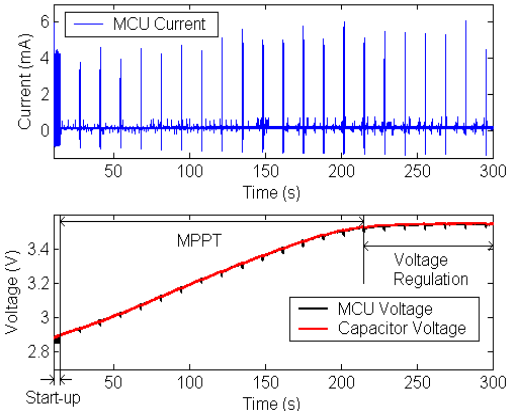

Figure 9. The measured MCU current and the output voltages

Figure 10 compares the maximal available power from the piezoelectric cantilever generator and the power extracted by our power management circuit. The maximum available power is measured as the power delivered to the optimal resistive load (of a given vibration frequency) connected directly to the piezoelectric generator, and the extracted power of our power management circuit is the power delivered to the supercapacitor while charging. The maximum available power of the piezoelectric generator under the acceleration of 0.5*g* is about 6.6 mW at the resonant frequency of 44 Hz. Our circuit harvests 3.5 mW, whose efficiency is about 53%. Some competing circuits report over 60% of efficiency in [6] under the acceleration of 0.5*g* (rms), and below 40% in [5] for the same amount of input power. However, direct comparison of those designs with ours should be judicious due to different environments. For example, [6] does not have a feedback controller, which attributes a substantial power consumption as described below. The circuit in [5] can manage input power as high as 50 mW, which results in a relatively low efficiency for low input power.

A breakdown of power losses at the resonant frequency of 44 Hz is shown in Figure 11. The power dissipation of the controller (specifically the MCU) and the diode are two major sources for the power loss and account for 64% of the total power loss. The next two sources of power losses are attributed to the inductor and the rectifier, especially their conduction losses.

VI. Conclusion

A self-powered power management circuit based on a DCM buck-boost converter is presented. An ultra-low power MCU is adopted for both the MPPT and the output voltage regulation. Experimental results indicate that the proposed system can harvest up to 3.5 mW power under 0.5*g* (rms) base acceleration for a piezoelectric cantilever and achieves 53% of the efficiency at the frequency. The sources of power losses are analyzed, and a breakdown of measured power losses is presented. Future works include further improvement of power efficiency and development of the efficient power management system in a monolithic IC.

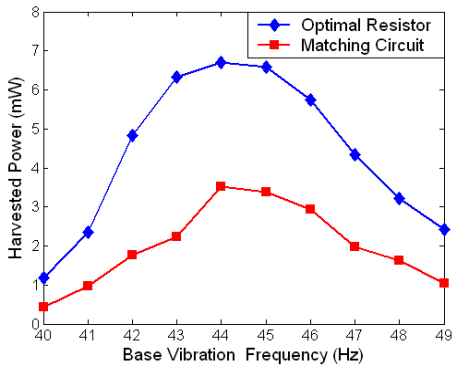

Figure 10. Average power harvested by optimal resistors and the proposed circuit.

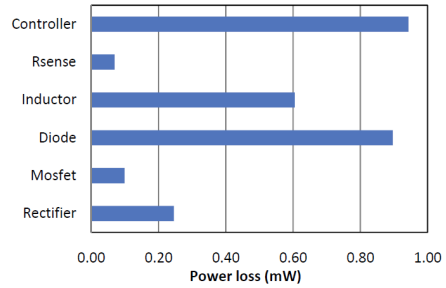

Figure 11. Power loss breakdown.

Acknowledgment

The authors gratefully acknowledge the support of the U.S. Department of Commerce, National Institute of Standards and Technology, Technology Innovation Program, Cooperative Agreement Number 70NANB9H9007.

References

[1] N. S. Hudak and G. G. Amatucci, "Small-scale energy harvesting through thermoelectric, vibration, and radiofrequency power conversion," Journal of Applied Physics, vol. 103, pp. 101301-1, 2008.

[2] C. O. Mathuna, T. O'Donnell, R. V. Martinez-Catala, J. Rohan, and B. O'Flynn, "Energy scavenging for long-term deployable wireless sensor networks," Talanta, vol. 75, pp. 613-623, 2008.

[3] S. Roundy, E. S. Leland, J. Baker, E. Carleton, E. Reilly, E. Lai, B. Otis, J. M. Rabaey, P. K. Wright, and V. Sundararajan, "Improving power output for vibration-based energy scavengers," IEEE Pervasive Computing, vol. 4, pp. 28-36, 2005.

[4] G. K. Ottman, H. F. Hofmann, A. C. Bhatt, and G. A. Lesieutre, "Adaptive piezoelectric energy harvesting circuit for wireless remote power supply," IEEE Transactions on Power Electronics, vol. 17, pp. 669-676, 2002.

[5] G. K. Ottman, H. F. Hofmann, and G. A. Lesieutre, "Optimized piezoelectric energy harvesting circuit using step-down converter in discontinuous conduction mode," *IEEE Transactions on Power Electronics,* vol. 18, pp. 696-703, 2003.

[6] E. Lefeuvre, D. Audigier, C. Richard, and D. Guyomar, "Buck-boost converter for sensorless power optimization of piezoelectric energy harvester," IEEE Transactions on Power Electronics, vol. 22, pp. 2018-25, 2007.

[7] T. Zaitsu, O. Ohnishi, T. Inoue, M. Shoyama, T. Ninomiya, F. C. Lee, and G. C. Hua, "Piezoelectric transformer operating in thickness extensional vibration and its application to switching converter," in Power Electronics Specialists Conference, PESC '94 Record., 25th Annual IEEE, 1994, pp. 585-589 vol.1.

[8] P. Joung-hu, C. Sungjin, L. Sangmin, and B. H. Cho, "Gain-adjustment Technique for Resonant Power Converters with Piezoelectric Transformer," in Power Electronics Specialists Conference, 2007. PESC 2007. IEEE, 2007, pp. 2549-2553.

[9] F. Dianbo, L. Ya, F. C. Lee, and X. Ming, "A Novel Driving Scheme for Synchronous Rectifiers in LLC Resonant Converters," Power Electronics, IEEE Transactions on, vol. 24, pp. 1321-1329, 2009.

[10] C. Richard, D. Guyomar, D. Audigier, and G. Ching, "Semi-passive damping using continuous switching of a piezoelectric device," in Proceedings of SPIE - The International Society for Optical Engineering, 1999, pp. 104-111.

[11] D. Guyomar, A. Badel, E. Lefeuvre, and C. Richard, "Toward energy harvesting using active materials and conversion improvement by nonlinear processing," IEEE Transactions on Ultrasonics, Ferroelectrics and Frequency Control , vol. 52, pp. 584-595, 2005.

[12] S. Xu, K. D. T. Ngo, T. Nishida, C. Gyo-Bum, and A. Sharma, "Converter and controller for micro-power energy harvesting," in IEEE Applied Power Electronics Conference and Exposition, 2005, pp. 226-230 Vol. 1.

[13] A. Badel, A. Benayad, E. Lefeuvre, L. Lebrun, C. Richard, and D. Guyomar, "Single crystals and nonlinear process for outstanding vibration-powered electrical generators," Ultrasonics, Ferroelectrics and Frequency Control, IEEE Transactions on, vol. 53, pp. 673-684, 2006.

[14] S. Roundy and P. K. Wright, "A piezoelectric vibration based generator for wireless electronics," Smart Materials and Structures, vol. 13, pp. 1131-1142, 2004.

[15] N. G. Elvin and A. A. Elvin, "A general equivalent circuit model for piezoelectric generators," Journal of Intelligent Material Systems and Structures, vol. 20, pp. 3-9, 2009.

[16] W. Erickson and D. Maksimovic, "Fundamentals of Power Electronics," Norwell, MA: Kluwer, 2001.

[17] O. Wasynczuk, "Dynamic behavior of a class of photovoltaic power systems," IEEE transactions on power apparatus and systems, vol. PAS-102, pp. 3031-3037, 1983.

[18] N. Femia, G. Petrone, G. Spagnuolo, and M. Vitelli, "Optimization of perturb and observe maximum power point tracking method," IEEE Transactions on Power Electronics, vol. 20, pp. 963-973, 2005.